The Effect of Hole Transport Material Pore Filling on Photovoltaic Performance in Solid-State Dye-Sensitized Solar Cells

*John Melas-Kyriazi, I-Kang Ding, Arianna Marchioro, Angela Punzi, Brian E. Hardin, George F. Burkhard, Nicolas Tétreault, Michael Grätzel, Jacques-E. Moser, and Michael D. McGehee**

A detailed investigation of the effect of hole transport material (HTM) pore filling on the photovoltaic performance of solid-state dye-sensitized solar cells (ss-DSCs) and the specific mechanisms involved is reported. It is demonstrated that the efficiency and photovoltaic characteristics of ss-DSCs improve with the pore filling fraction (PFF) of the HTM, 2,2',7,7'-tetrakis-(*N*, *N* -di- *p* -methoxyphenylamine)9,9'-spirobifluorene(spiro-OMeTAD). The mechanisms through which the improvement of photovoltaic characteristics takes place were studied with transient absorption spectroscopy and transient photovoltage/photocurrent measurements. It is shown that as the spiro-OMeTAD PFF is increased from 26% to 65%, there is a higher hole injection efficiency from dye cations to spiro-OMeTAD because more dye molecules are covered with spiro-OMeTAD, an order-of-magnitude slower recombination rate because holes can diffuse further away from the dye/HTM interface, and a 50% higher ambipolar diffusion coefficient due to an improved percolation network. Device simulations predict that if 100% PFF could be achieved for thicker devices, the efficiency of ss-DSCs using a conventional ruthenium-dye would increase by 25% beyond its current value.

1. Introduction

Photovoltaic cells have emerged as a promising source of clean energy to meet rising concerns for global climate change.[1] Dye-sensitized solar cells (DSCs) have received sustained attention as one of the most promising photovoltaic technologies, both for their low-cost materials and high power conversion efficiencies.[2,3] Devices using liquid electrolytes have shown efficiencies surpassing 11%.[4] Liquid-electrolyte DSCs usually have an open-circuit voltage less than 800 mV, limited by the energy offset between the conduction band of TiO_2 and the potential of the redox couple.[5] Solid-state dye-sensitized solar cells (ss-DSCs) use solid-state hole transport materials (HTMs) such as 2,2',7,7'-tetrakis-(*N*,*N*-di-*p*-methoxyphenylamine)9,9'-spirobifluorene (spiro-OMeTAD) to replace liquid electrolytes.[6,7] They offer a viable pathway to higher efficiency because the open-circuit voltage can be tuned by adjusting the highest occupied molecular orbital (HOMO) of the HTM. The use of solid-state HTMs also solves potential leakage and corrosion problems associated with liquid electrolytes.

State-of-the-art ss-DSCs using films of mesoporous TiO_2 and spiro-OMeTAD as a HTM have just recently reached 6% efficiency[8] and are optimized at a film thickness of 2 μm. Cells built with thicker films absorb more light but exhibit poor charge collection. This has been attributed to short diffusion lengths of charge carriers inside the cell at operating voltages[9],[10] and to the incomplete filling of TiO_2 pores with spiro-OMeTAD.[11] The pore filling of spiro-OMeTAD has long been suggested as an important factor in ss-DSC performance,[12] but the mechanism behind its impact on device efficiency has not been thoroughly studied until this point. Recently, we have developed techniques to accurately measure the pore filling fraction (PFF), or the percentage of TiO_2 pore volume occupied by spiro-OMeTAD.[13] Currently, the PFF is limited to approximately 65% in state-of-the-art 2-μm-thick devices, and high PFFs are particularly difficult to achieve with thicker TiO_2 films.[10,13,14] Improving the PFF is an active research effort in the field.

Here we report a detailed investigation of the effect of pore filling on ss-DSC performance and device physics. We varied the concentration of spiro-OMeTAD solution used for infiltration and fabricated ss-DSCs at four different PFFs (26%, 39%, 52%, and 65%). Our cells were fabricated following standard procedure using 2-μm-thick TiO_2 films sensitized with Z907, an amphiphilic polypyridyl ruthenium complex commonly

J. Melas-Kyriazi, I.-K. Ding, Dr. B. E. Hardin, Dr. G. F. Burkhard, Prof. M. D. McGehee
Department of Materials Science and Engineering
Stanford University
Stanford, CA 94305, USA
E-mail: mmcgehee@stanford.edu
A. Marchioro, Dr. A. Punzi, Dr. N. Tétreault, Prof. M. Grätzel, Prof. J.-E. Moser
Institute of Chemical Sciences and Engineering
École Polytechnique Fédérale de Lausanne
1015 Lausanne, Switzerland

DOI: 10.1002/aenm.201100046

used in ss-DSCs.[15] Our findings show that increasing the PFF from 26% to 65% improves the hole injection efficiency from the dye cation to spiro-OMeTAD, significantly increases the recombination lifetime of charge carriers, and enhances hole transport through spiro-OMeTAD. Based on the mechanisms we have observed, we calculate how much increasing the PFF past the current value of 65% should improve the performance of devices and allow the optimal TiO_2 thickness to increase.

2. Results and Discussion

2.1. Photovoltaic Performance

The photovoltaic characteristics of ss-DSCs with varying PFFs are shown in **Figure 1**. Between 26% and 65% PFF, the power conversion efficiency (η) of our devices improved by a factor of 3 due to consistent increases in short-circuit current (J_{sc}), open-circuit voltage (V_{oc}), and fill factor (FF). The strongest improvement was seen in the J_{sc}, which increased on average by about 2.2x. We attribute this effect to both improved hole injection from dye cation to spiro-OMeTAD and increased charge collection efficiency. The V_{oc} improved by almost 100 mV, suggesting a significant increase in recombination lifetime, which we demonstrate in Section 2.3.

2.2. Hole Injection from Dye Cations to Spiro-OMeTAD

During ss-DSC operation, a dye molecule excited by the absorption of an incident photon rapidly injects an electron into the TiO_2 conduction band. The dye cation can then be regenerated either via hole injection from dye to spiro-OMeTAD or through direct recombination with an electron in TiO_2. Previous work has shown that hole injection from dye to spiro-OMeTAD takes place over a range of time scales spanning from picoseconds to nanoseconds[16,17] and that dye regeneration through recombination with electrons in TiO_2 is significantly slower, on the order of hundreds of microseconds for Z907.[18] Since hole injection can be orders of magnitude faster than the competing recombination reaction, we expect the main limitation on the hole injection efficiency results from incomplete dye coverage with spiro-OMeTAD, which strands holes on dye molecules until they recombine with electrons in TiO_2.

The effect of pore filling on hole injection has not yet been explicitly examined, although Kroeze et. al. postulated from their study of different HTMs that the PFF may strongly impact the hole injection efficiency (defined as the fraction of photogenerated holes that are successfully injected from dye cations to spiro-OMeTAD).[16] In a previous study, we estimated that approximately 49% PFF is required to provide a monolayer of dye coverage with spiro-OMeTAD, assuming 20 nm spherical TiO_2 pores and conformal coating of spiro-OMeTAD on adsorbed Z907.[13] Below this sub-monolayer threshold, a significant fraction of dye molecules are not in contact with spiro-OMeTAD. In reality, a perfectly conformal coating of spiro-OMeTAD in the TiO_2 pores is highly unlikely, even above this threshold. Therefore, some fraction of the dye molecules will not be covered with spiro-OMeTAD, especially in smaller pores where the diffusion of spiro-OMeTAD molecules is slower during deposition. We depict both "low" pore filling (sub-monolayer) and "high" pore filling scenarios in **Figure 2**. Based on this model, we expect that increasing the PFF will improve dye coverage with spiro-OMeTAD and increase the hole injection efficiency.

We studied hole injection in samples with four different PFFs (26%, 39%, 52%, and 65%) using transient absorption spectroscopy.[16,19] The experiment was performed with a pump wavelength of 532 nm and a probe wavelength of 520 nm. In the absence of spiro-OMeTAD, the pump beam excites the Z907 dye, resulting in electron injection into the TiO_2 conduction band; therefore, photobleaching of the ground state dye absorption is observed. In films that contain spiro-OMeTAD, an increase in absorption at the probe wavelength is observed due to both reduced photobleaching of the dye and increased absorption from spiro-OMeTAD$^+$ resulting from hole injection from the dye cation. The probe wavelength was specifically chosen so that there would be negligible absorption from the dye cation and unoxidized spiro-OMeTAD. It is well known that spiro-OMeTAD does not absorb significantly at wavelengths longer than 450 nm.[20] Photoinduced absorption studies have shown that TiO_2 sensitized with the ruthenium-based dye N3, a dye with very similar structural characteristics to Z907, exhibits strong bleaching at the probe wavelength, suggesting that dye cation absorption at this wavelength is far weaker than absorption from the dye ground state in this family of dyes.[21] The hole injection efficiency (η_{hole_inj}) can then be determined by

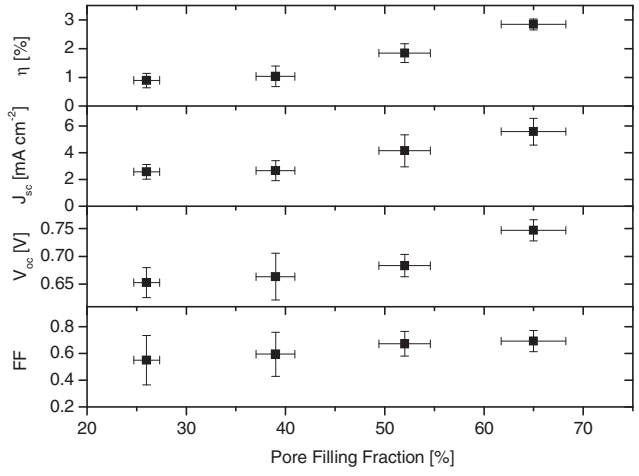

Figure 1. Current-voltage (I–V) characteristics for 2-μm-thick devices at 1-sun illumination intensity (100 mW cm^{-2}).

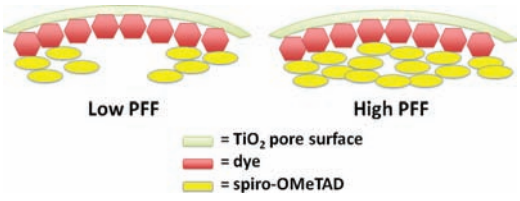

Figure 2. Schematic illustration showing the improvement of dye coverage with spiro-OMeTAD between low and high PFFs.

comparing the change in optical density after a pump pulse in samples with and without spiro-OMeTAD (ΔOD_{w_spiro} and ΔOD_{wo_spiro}, respectively) and using the equation:

$$\Delta OD_{w\_spiro} = \Delta OD_{wo\_spiro} \cdot (1 - \eta_{hole\_inj}) - \Delta OD_{wo\_spiro} \cdot \eta_{hole\_inj} \cdot \frac{\varepsilon_{spiro^+}}{\varepsilon_{Z907}} \quad (1)$$

ε_{spiro}^+ and ε_{Z907} are the absorption coefficients of spiro-OMeTAD$^+$ (18,700 M^{-1} cm^{-1})[17] and the Z907 ground state (12,000 M^{-1} cm^{-1})[22] at 520 nm, respectively. The first term on the right side of Equation 1 shows how ΔOD_{w_spiro} drops as hole injection to spiro-OMeTAD from the dye cation reduces the ground state bleach. The second term accounts for the absorption by spiro-OMeTAD$^+$ that replaces bleaching in the dye as holes transfer to spiro-OMeTAD. A detailed derivation of Equation 1 is shown in the supporting information. For our samples, we used optical densities averaged between the rise time of the detection system (~40 µs) and the onset of the recombination reaction (~100 µs).[18]

Figure 3a shows ΔOD as a function of time in samples with and without spiro-OMeTAD, and Figure 3b shows that the hole injection efficiency significantly increases with higher PFF, as expected. Between 26% and 65% PFF, there is an increase in hole injection efficiency of approximately 1.65x, from 57% to 94%. The hole injection efficiency value of 94% measured for 65% PFF is slightly higher than but within experimental error of the value of 90% measured by Kroeze et al.[16] Figure 1 showed that the J_{sc} increased by about 2.2× between our 26% and 65% PFF devices. The J_{sc} is directly proportional to the hole injection efficiency, so the increase in hole injection efficiency with PFF that we have demonstrated accounts for a significant portion of this gain. We note that there has recently been renewed discussion on the uncertainty of absorption coefficients (ε_{spiro}^+ and ε_{Z907}) caused by the Stark effect or measurement errors,[23–25] which could shift the hole injection efficiency values shown in Figure 3b. Nonetheless, the trend of higher PFF resulting in higher hole injection efficiency remains valid.

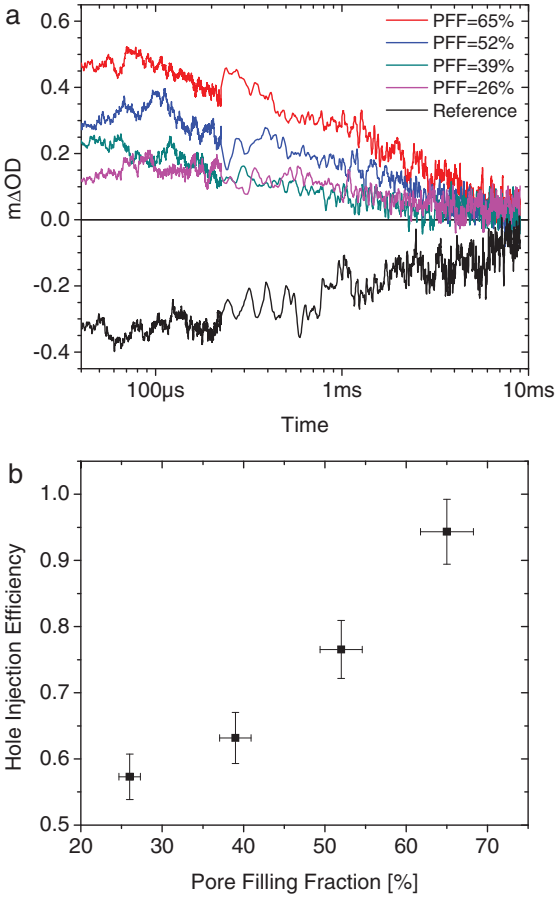

Figure 3. a) Change in optical density at 520 nm after excitation at 532 nm for 2-µm-thick devices with different spiro-OMeTAD PFFs and one reference device with no spiro-OMeTAD; b) calculated hole injection efficiencies vs. PFF.

Equation 1 is valid under the assumption that the formation of the spiro-OMeTAD$^+$ species following hole injection is complete within the rise time of the detection system (40 µs). Our technique might slightly underestimate hole injection efficiency in the case that mechanisms slower than 40 µs account for a significant fraction of hole injection. Normally, we expect hole injection to be complete after approximately 10 ns.[17] However, in the case of low PFF samples, there may be many dye molecules that are not touching spiro-OMeTAD and cannot directly inject their holes. One of the potential slower injection mechanisms is via lateral "hole-hopping" between dye molecules,[17,26] where a hole on one dye cation is transferred to another dye molecule that is contacting spiro-OMeTAD. Wang et al. measured the hole diffusion coefficient on a self-assembled monolayer of Z907 to be approximately 4.1×10^{-9} cm^2 s^{-1}.[26] Using this value, we can calculate the expected displacement of holes from their original dye molecules at any time after dye cation formation using a simple diffusion model. After 180 µs, which is approximately the decay half-time of the competing recombination process between electrons in TiO_2 and Z907 cations,[18] a hole will have diffused about 9 nm, spanning approximately seven Z907 molecules.[27] Therefore, we expect that some dye cations that are not directly touching spiro-OMeTAD will be able to transfer their hole through this "hole-hopping" process and avoid recombination with electrons in TiO_2. However, no significant increase in absorption in our measurements between 40 and 100 µs was observed, suggesting that hole injection happens faster than 40 µs, even for sub-monolayer systems such as 26% and 39% PFF.

2.3. Recombination Between Electrons in TiO_2 and Holes in Spiro-OMeTAD

Following charge separation at the TiO_2/dye/spiro-OMeTAD interface, recombination between electrons in TiO_2 and holes in spiro-OMeTAD becomes the dominant loss mechanism in ss-DSCs. Recombination is thought to occur via quantum mechanical tunneling of electrons from TiO_2 through the dye to recombine with holes in spiro-OMeTAD.[28] As we increase the amount of spiro-OMeTAD in the TiO_2 pores, we slow down recombination by allowing holes to diffuse away from the pore surface, thereby increasing the average spatial separation between electrons in TiO_2 and holes in spiro-OMeTAD as depicted schematically in **Figure 4**.

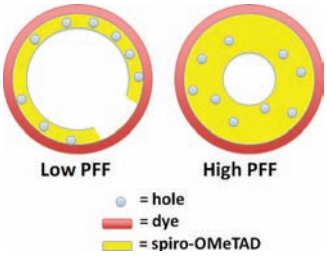

Figure 4. Schematic diagram showing the effect of the PFF on the spatial separation of holes from the dye-coated TiO_2 pore surface. Sub-monolayer coverage of dye molecules with HTM is shown in the case of low PFF. Real pores are not perfectly spherical as shown here.

To directly quantify the effect of pore filling on recombination, we measured the recombination lifetime (inverse of the recombination rate constant) in our devices using transient photovoltage measurements, as described previously.[10,29] **Figure 5** shows the measured recombination lifetimes under short-circuit conditions. A strong linear correlation between the PFF and the recombination lifetime was observed, with roughly an order of magnitude increase between 26% and 65% PFF.

The recombination lifetime directly affects the open-circuit voltage (V_{oc}) of a device. Using a model derived by Snaith et al. for ss-DSCs[28] we expect the V_{oc} to scale with τ_{rec} according to Equation 2, where the constant V_0 depends on a variety of factors, d is the film thickness, α is the average absorption coefficient of the film, τ_0 is a time constant, and d_0 is a length constant (a detailed derivation is shown in the supporting information):

$$V_{OC} = V_0 + \frac{2kT}{q}(\ln(\tau_{rec}/\tau_0) - 2\ln(d/d_0) + \ln(1 - e^{-\alpha d})) \quad (2)$$

Using our obtained recombination lifetimes for the 26% and 65% PFF cells, from Equation 2 we expect a 99 mV increase in V_{oc} at room temperature in this pore filling range, which is well within experimental error of the actual average improvement of 94 mV that we observed. We expect that enhancing the PFF past 65% will continue to increase the average spatial separation of opposite charge carriers in ss-DSCs, and thereby further increase the recombination lifetime.

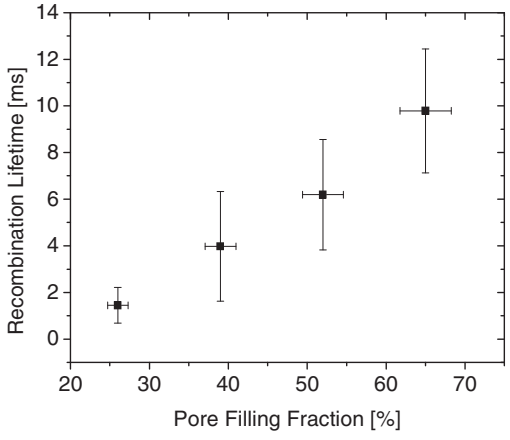

Figure 5. Recombination lifetime vs. PFF at short-circuit (V = 0) for 2-µm-thick devices, obtained through transient photovoltage measurements at 100 mW cm^{-2} white light intensity.

2.4. Ambipolar Charge Transport

For effective charge collection in ss-DSCs, injected charges must reach their respective electrodes before recombination. Therefore, efficient charge transport is crucial to device performance. Charge transport in DSCs is known to be a process of ambipolar diffusion, where electrons in TiO_2 and holes in the hole transport medium have different charge carrier mobilities but are extracted from the device at the same rate.[30] An ambipolar diffusion coefficient (D_{amb}) describes the diffusion of both electrons and holes (where n and p are the concentration of electrons and holes respectively, and D_n and D_p are the diffusion coefficients of electrons and holes respectively):

$$D_{amb} = \frac{(n+p)}{(n/D_p) + (p/D_n)} \quad (3)$$

As we increase the amount of spiro-OMeTAD inside the pores, we provide a less "torturous" route for holes to diffuse to the device electrodes.[31] According to percolation theory, which has been applied to similar systems such as electrons diffusing in mesoporous TiO_2,[32] an increase in the fraction of pore space occupied by spiro-OMeTAD should increase D_p, which would boost D_{amb}. We directly measured D_{amb} in our devices with different PFFs through transient photocurrent measurements. The photocurrent decay time constant (τ_j) extracted from a transient photocurrent measurement is considered to represent the sum of the recombination rate and the charge transport rate:[29]

$$\frac{1}{\tau_j} = \frac{1}{\tau_{rec}} + \frac{1}{\tau_{trans}} \quad (4)$$

Once τ_j and τ_{rec} were measured at a particular potential, the charge transport lifetime (τ_{trans}) was extracted, and D_{amb} was calculated as per the literature[10] (where d is the device thickness):

$$D_{amb} = \frac{d^2}{2.35 \cdot \tau_{trans}} \quad (5)$$

We found a small but statistically significant improvement in D_{amb} at V = 0 with pore filling, with an increase of approximately 1.5× between 26% and 65% PFF (**Figure 6**).

D_{amb} only changes by a small amount with pore filling because it is primarily limited by electron transport in TiO_2,[31] and the diffusion of electrons in TiO_2 is not significantly impacted by the PFF. Therefore, we expect any further gains in D_{amb} with pore filling past 65% to be small. Below 26% PFF, we expect D_{amb} to quickly decrease as the hole conduction pathway reaches a critical percolation threshold[32] below which transport is no longer possible. In our experience, ss-DSCs using spiro-OMeTAD cease to function with less than about 15% PFF, almost certainly due to this effect. It should be noted that ss-DSCs using semiconducting polymers (such as P3HT[33] or PEDOT[34]) may exhibit higher D_{amb} at lower PFFs because of higher charge carrier mobilities and lower percolation thresholds associated with these polymers.

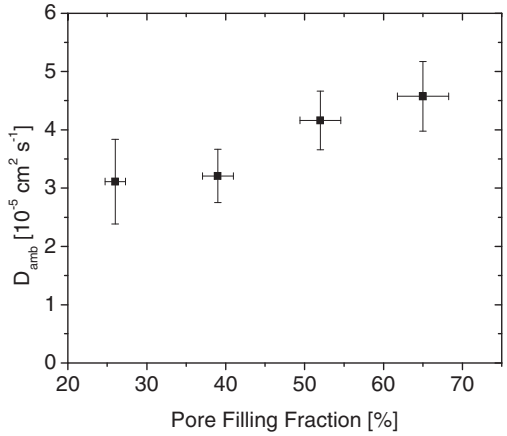

Figure 6. Ambipolar diffusion coefficient vs. PFF at short-circuit (V = 0) for 2-µm-thick devices, obtained through transient photovoltage and photocurrent measurements at 100 mW cm^{-2} white light intensity.

2.5. Charge Collection Efficiency and Diffusion Lengths

Having quantitatively investigated both the processes of charge transport and recombination, we directly calculated the effective diffusion lengths and charge collection efficiencies in our devices. The effective diffusion length (L_D), or average distance traveled by charge carriers before recombination, was calculated from the following equation:

$$L_D = \sqrt{D_{amb} \cdot \tau_{rec}} \quad (6)$$

In light of recent debate in the literature as to how to properly measure the diffusion length in DSCs,[35 – 37] our analysis focuses mostly on charge collection efficiency. The charge collection efficiency (η_{cc}) represents the percentage of successfully injected charges that reach the device electrodes, and was calculated as follows:[38]

$$\eta_{cc} = \frac{1}{1 + (\tau_{trans}/\tau_{rec})} \quad (7)$$

Diffusion lengths and charge collection efficiencies at V = 0 for our devices are shown in **Figure 7**a and 7b, respectively.

There was a strong linear relationship between L_D at V = 0 and the PFF in our cells, whereas the charge collection efficiency rapidly improved from 68% at 26% PFF and then saturated, achieving 96% at 65% PFF. The charge collection efficiency can also be used to calculate the internal quantum efficiency (IQE) of a DSC, which is the product of the electron injection efficiency ($\eta_{electron\_inj}$), hole injection efficiency (η_{hole_inj}), and charge collection efficiency (η_{cc}):

$$IQE = \eta_{electron\_inj} \cdot \eta_{hole\_inj} \cdot \eta_{cc} \quad (8)$$

The J_{sc} is proportional to the *IQE*, and therefore also to the charge collection and hole injection efficiencies. We observed an average gain in J_{sc} of 2.2x between 26% and 65% PFF (Figure 1), which was significantly higher than the average improvement in charge collection efficiency of 1.4x (Figure 7b).

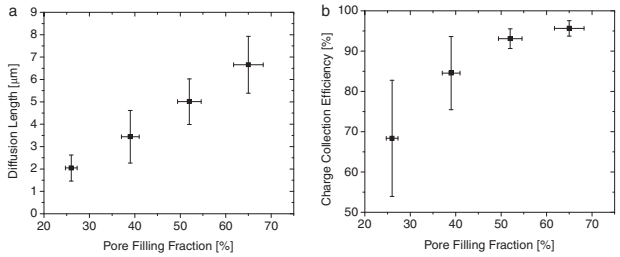

Figure 7. a) Calculated diffusion lengths and b) charge collection efficiencies for for 2-µm-thick devices at V = 0 at 100 mW cm^{-2} white light intensity.

We assume that the electron injection efficiency was constant throughout our samples, and attribute any additional gains in J_{sc}, after accounting for the charge collection efficiency, to an improvement in the hole injection efficiency. Therefore, based on our charge collection efficiency and J_{sc} data, we estimate that the hole injection efficiency improved by a factor of 1.55 between 26% and 65% PFF. This is within experimental error of the improvement of 1.65 in hole injection efficiency that we measured in this range (Figure 3b).

Even though charge collection was nearly unity (96%) for optimized (2-µm-thick 65% PFF) ss-DSCs, this would not be the case for thicker films, even if we were able to maintain 65% PFF. Equation 5 shows that the transport lifetime (τ_{trans}) is proportional to the square of the film thickness at a constant diffusion coefficient. Thus, even with constant pore filling, charge collection efficiency would significantly decrease with a thicker film. As discussed before, we expect that increasing the PFF past 65% will continue to increase recombination lifetimes, which would help to boost charge collection for thicker films.

2.6. Future Device Performance with Enhanced Pore Filling

In this materials system, further enhancement of pore filling is crucial to efficient performance in devices thicker than 2 µm. The highest PFF we achieved in this project was approximately 65% due to limitations with solution-based deposition.[14] However, it is instructive to consider the extent of the efficiency improvement if the PFF could be increased to 100% regardless of the TiO_2 film thickness. The efficiency improvement can be predicted quantitatively by calculating how the V_{oc} and J_{sc} are affected by the change in device thickness and recombination lifetime.

There are several assumptions involved in our model. First, we assume that the primary effect of increasing the PFF from 65% to 100% is to increase the recombination lifetime, which is strongly dependent on the choice of dye and HTM (Z907 and spiro-OMeTAD for this study), and that the two parameters have a linear relationship. From the linear fit of Figure 5, we assume that increasing the PFF from 65% to 100% will increase the recombination lifetime by 70% to 16.8 ms. We further assume that increasing the PFF will not help hole injection because nearly all dye molecules are well covered by spiro-OMeTAD at 65% PFF, and that the ambipolar diffusion coefficient for 100% PFF is the same as at 65% PFF because the ambipolar diffusion

coefficient at high pore filling is primarily limited by electron transport in TiO_2.

Using Equation 2, we calculated the V_{oc} as a function of the recombination lifetime (τ_{rec}) and device thickness (d). V_0 was calculated by substituting in the known values of the other parameters from a reference device. The short-circuit photocurrent (J_{sc}) can be obtained by integrating the product of EQE and solar illumination intensity against wavelength. The EQE for ss-DSCs is product of the absorption ($\eta_{abs}(\lambda)$) and IQE (Equation 9):

$$EQE(\lambda) = \eta_{abs}(\lambda) \cdot \eta_{electron\_injection} \cdot \eta_{hole\_injection} \cdot \eta_{cc} \quad (9)$$

For devices with different thicknesses, $\eta_{abs}(\lambda)$ can be calculated by Beer's law, and η_{cc} can be calculated using Equations 5 and 7. The extinction coefficient for each wavelength was obtained by measuring the absorption of the active layer with an integrating sphere.[39] The product of electron injection efficiency and hole injection efficiency for our reference device was estimated to be 0.84 by independently measuring the IQE and charge collection efficiency. Finally, the J_{sc} was obtained by integrating the product of EQE and solar illumination intensity.

The modeled charge collection efficiency, J_{sc}, V_{oc} and power conversion efficiency as a function of TiO_2 film thicknesses are shown in **Figure 8**. The fill factor was assumed to be 0.7 and independent of thickness. Two different scenarios are considered: PFF = 65%, and PFF = 100%. It should be noted that both are "ideal-case" scenarios, as in reality, PFF decreases with increasing TiO_2 film thicknesses.[10,13] We can see from Figure 8 that as thickness goes up, the J_{sc} increases and plateaus (due to increasing light absorption but decreasing charge collection efficiency) and the V_{oc} consistently decreases. The effect of increasing thickness on power conversion efficiency is as follows: the efficiency increases early on due to improved light absorption, but eventually reaches a plateau and starts dropping again as the charge collection efficiency decreases and V_{oc} losses become significant. The thickness at which the efficiency reaches a plateau is larger at higher pore filling. If 100% PFF could be realized on a thick film, an optimized device (5-μm-thick, 100% PFF) would be 4.0% efficient, which is 25% higher than the 3.2%-efficient reference device used in this model (2-μm-thick, 65% PFF). It should be noted that the calculation above is based on ss-DSCs with Z907 dye; organic dyes with higher extinction coefficients will make the J_{sc} saturate at thinner thicknesses, but increasing the PFF should still benefit the power conversion efficiency because of the increase in η_{cc} and V_{oc}. Developing techniques for further improving the PFF is an active area of research.[14,40]

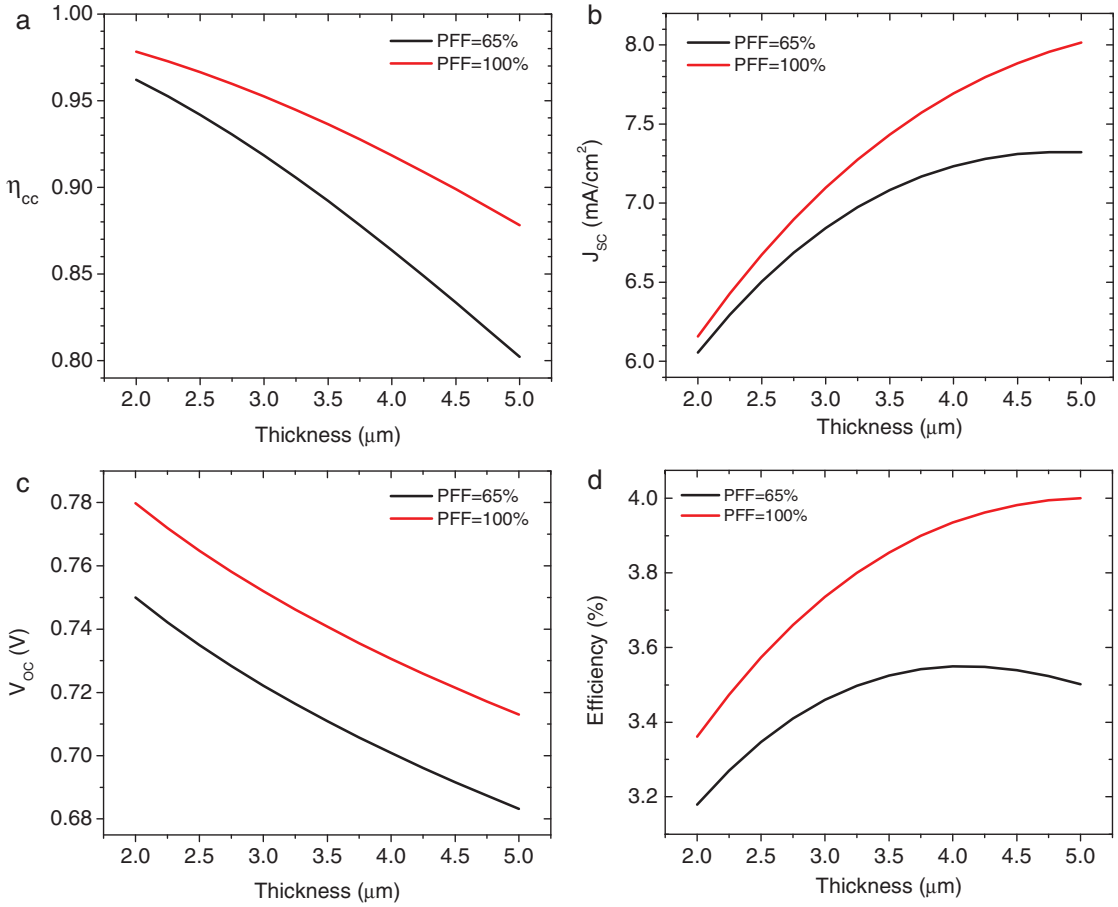

Figure 8. Modeled device parameters for Z907/spiro-OMeTAD system as a function of TiO_2 thickness for two different scenarios: PFF = 65% (black line), and PFF = 100% (red line). a) charge collection efficiency, η_{cc}; b) short-circuit photocurrent, J_{sc}; c) open-circuit voltage, V_{oc}; d) power conversion efficiency.

3. Conclusions

The effect of hole transport material pore filling on device physics in solid-state dye-sensitized solar cells was quantitatively investigated for the first time using Z907-sensitized ss-DSCs and the HTM spiro-OMeTAD. The photovoltaic performance of our 2-µm-thick devices correlated strongly with the PFF, with a 3-fold increase in efficiency between devices with 26% and 65% PFF. Using a combination of transient absorption spectroscopy and transient photovoltage/photocurrent measurements, we showed that increasing the PFF impacts device physics in the following ways: 1) improving the coverage of dye with spiro-OMeTAD, yielding a higher charge injection efficiency; 2) reducing the concentration of holes at the TiO_2/dye/spiro-OMeTAD interface, giving a higher recombination lifetime; and 3) improving the percolation pathway of holes in spiro-OMeTAD, increasing the ambipolar diffusion coefficient for charges in the device. Using the data we collected, we predicted the performance of thicker Z907-sensitized ss-DSCs with 65% and 100% PFF of spiro-OMeTAD. Our model suggests that, due to further increases in the recombination lifetime, with 100% PFF the efficiency-optimized film thickness would significantly increase from 2 to 5 µm, and the efficiency would improve by about 25% from its current value due to enhanced light absorption.

This work has broad implications for ss-DSC development, as the qualitative trends we have proposed and demonstrated with spiro-OMeTAD in this study can likely be extended to other HTMs. Furthermore, the device modeling strategy presented here, which focuses on decomposing the EQE and V_{oc} as a function of experimentally determined parameters, is applicable to any DSC system. The methods used in this study to determine the hole injection and charge collection efficiencies of devices are also widely transferable.

The development of >10% efficient ss-DSCs will most likely require using a variety of parallel strategies to increase light absorption and reduce recombination. We identify increasing the PFF as one promising approach that is complementary to a number of others, including developing high-extinction-coefficient and broad-absorbing dyes[7,8] and/or light absorbing hole transport materials,[33] using energy relay concepts to broaden absorption spectra,[41–43] using plasmonic effects to increase light absorption,[44,45] and designing new dyes, HTMs, and co-adsorbents that reduce recombination rates.[46,47] We believe that the development of new HTMs and deposition techniques that can achieve near-unity pore filling in TiO_2 [14] will play a crucial role in optimizing future ss-DSCs.

4. Experimental Section

Cell Fabrication: Fluorine doped tin oxide coated glass (Pilkington TEC 15) was patterned through etching with zinc powder and 4 M HCl, and then cleaned by scrubbing with 2% Helmanex detergent in water followed by rinsing with acetone and ethanol. A thin (approximately 100 nm) compact layer of TiO_2 was deposited through spray pyrolysis of diluted titanium diisopropoxide bis(acetylacetonate) in ethanol, using oxygen as a carrier gas. 2-µm-thick mesoporous TiO_2 films (roughly 0.7 cm^2) were screen printed on top of the compact layer using a widely available TiO_2 nanoparticle paste (Dyesol 18-NRT), and sintered at 500 °C. The samples were treated with 0.02 M $TiCl_4$ at room temperature for 6 hours, followed by rinsing with water and heating again to 500 °C. At approximately 80° C the cells were dipped into Z907 dye (0.3 mM in 1:1 acetonitrile:tert-butyl alcohol) for 6 hours, and then rinsed with acetonitrile to remove excess dye. Spiro-OMeTAD was dissolved in chlorobenzene at a concentration of 180 mg/mL by heating for 30 minutes at 60 °C. Lithium bis(trifluoromethylsulfonyl)imide salt (Li-TSFI) dissolved in acetonitrile (170 mg/mL) was added to the spiro-OMeTAD solution at a ratio of 15 µL Li-TFSI solution: 72 mg of spiro-OMeTAD, and 4-*tert*-Butylpyridine (TBP) was added at a ratio of 7 µL TBP: 72 mg spiro-OMeTAD. The spiro-OMeTAD solution was then diluted with chlorobenzene to various other concentrations, but the ratio of spiro-OMeTAD to Li-TFI and TBP remained unchanged. The cells were spin coated with approximately 40 µL of spiro-OMeTAD solution at a rate of 2000 rpm for 30 seconds. 100 nm gold electrodes were thermally evaporated onto the cells. Gold was chosen for an electrode material because it forms a Schottky barrier with TiO_2 in ss-DSCs,[31] preventing a shunting route for electrons in the case where there is little or no spiro-OMeTAD blocking overlayer. The cells were each sealed with a glass slide heated onto a 25 µm Surlyn frame surrounding the cell active area. All cells were stored in the dark after fabrication. Each data point on Figures 1, 5, 6, and 7 represent the mean and standard deviation from 5 – 6 identical cells.

Pore Filling Quantification: The pore filling fractions reported in this study were calculated using previous work[13] that experimentally confirmed a model[10] relating the TiO_2 pore filling fraction to the spiro-OMeTAD spin coating concentration. Empirically, the relationship between the PFF and spiro-OMeTAD spin coating concentration is linear from 0 to 180 mg/mL for a cell of roughly 2 µm thickness, whereafter it saturates at a PFF of approximately 65%.[13,14] We refer to cells spin coated at 72 mg/mL, 108 mg/mL, 144 mg/mL, and 180 mg/mL as having 26%, 39%, 52%, and 65% pore filling respectively. A 5% relative standard deviation in the calculated PFF was estimated based on our experience.

Transient Photovoltage and Photocurrent Measurements: Transient photocurrent and photovoltage measurements were taken with the same physical setup as the one Snaith et al. used.[10] Cells were white light biased at 1 sun (100 mW cm^{-2}) with an array of white Lumiled diodes and pulsed with 50 ms square waves from four red LEDs. The red light pulse intensity was designed to give less than 5% perturbation in photovoltage at the cell's V_{oc} in order to ensure mono-exponential decay kinetics. Voltage and current across the cells were controlled and measured with a Keithley 2400 sourcemeter. For each transient photocurrent measurement, a fixed bias was held across the cell, and during the transient red light pulse the current output of the cell temporarily increased. After the light pulse the time constant (τ_j) of the ensuing mono-exponential photocurrent decay was measured. Similarly, for each transient photovoltage measurement, a fixed current was held through the cell, biasing the cell at a specific point on its current-voltage (I-V) curve, and the mono-exponential photovoltage decay following the transient pulse was due solely to the recombination of charges within the film.[10] Fitting this photovoltage decay yielded the recombination lifetime (τ_{rec}). After a 5 minute light soak at 1 sun, transient photocurrent and photovoltage measurements were taken at various bias points in 40 mV steps, scanning from V_{oc} to short circuit (V = 0), roughly a 15 minute process. Our analysis focused on lifetimes obtained at V = 0 since this is a convenient constant bias point for diverse samples. The transient red LED pulse intensity was kept constant for each of these measurements and between different cells. For transient photovoltage measurements, it became difficult to accurately enforce a bias near short circuit due to the typical flat shape of the photovoltaic current-voltage curve in that region, so the bias point closest to V = 0 was chosen to represent short circuit for each cell. This generally fell within approximately ±0.05 V of V = 0.

I–V Measurements: Cells were subjected to an additional 3 minute light soak at 1 sun directly before *I–V* measurements. *I–V* curves were taken with a Keithley 2400 sourcemeter, using an AM 1.5G solar simulator with a Xenon lamp calibrated with a reference silicon diode; a full description of this setup is given elsewhere.[48] The size of the mask used to test the cells was 0.1517 cm^2 (as measured by SEM). The cells had been characterized through transient measurements less than 12 hours prior to *I–V* testing.

Transient Absorption Spectroscopy: Transmission-mode transient absorption experiments were conducted using a frequency doubled,

Q-switched Nd:YAG laser (Spectra-Physics) as the excitation source (532 nm, 10 Hz rep. rate, and 5 ns pulse duration). The probe beam was comprised of a 100 W mercury lamp coupled into a monochromator with order-sorting filters. An identical monochromator (also with order sorting filters) was placed after the sample to reject stray light from the detector. The signal was acquired using a silicon photodiode with a home-built amplification/filtering system and was captured using a digital oscilloscope (Tektronix). High frequency noise was further removed using a Savitzky-Golay smoothing technique. Devices for transient absorption measurements were fabricated according to standard procedure[14] but without a metal electrode, and were sealed in a nitrogen chamber before characterization to avoid dye degradation in air. Each data point in Figure 3b represents one device, with the error bars representing the calculated instrument error.

Acknowledgements

J. M.-K. and I.-K. D. contributed equally to this work. This publication was partially based on work supported by the Center for Advanced Molecular Photovoltaics (Award No KUS-C1 – 015-21) made by King Abdullah University of Science and Technology (KAUST). A. M., A. P., N. T., M. G., and J.-E. M. are grateful to the Swiss National Science Foundation for financial support. We thank Dr. Robin Humphry-Baker for his experimental assistance with transient photovoltage/photocurrent measurements, Dr. Shaik M. Zakeeruddin for providing Z907 dye, Manuel Tschumi for fabricating TiO_2 films, and George Y. Margulis for providing absorption data used in Section 2.6.

Received: February 2, 2011
Revised: March 4, 2011
Published online: April 5, 2011

[1] M. I. Hoffert, K. Caldeira, G. Benford, D. R. Criswell, C. Green, H. Herzog, A. K. Jain, H. S. Kheshgi, K. S. Lackner, J. S. Lewis, H. D. Lightfoot, W. Manheimer, J. C. Mankins, M. E. Mauel, L. J. Perkins, M. E. Schlesinger, T. Volk, T. M. L. Wigley, *Science* **2002**, *298*, 981.
[2] M. Grätzel, *Inorg. Chem.* **2005**, *44*, 6841.
[3] B. O'Regan, M. Grätzel, *Nature* **1991**, *353*, 737.
[4] F. Gao, Y. Wang, D. Shi, J. Zhang, M. Wang, X. Jing, R. Humphry-Baker, P. Wang, S. M. Zakeeruddin, M. Grätzel, *J. Am. Chem. Soc.* **2008**, *130*, 10720.
[5] H. J. Snaith, *Adv. Funct. Mater.* **2010**, *20*, 13.
[6] U. Bach, D. Lupo, P. Comte, J. E. Moser, F. Weissörtel, J. Salbeck, H. Spreitzer, M. Grätzel, *Nature* **1998**, *395*, 583.
[7] J.-H. Yum, P. Chen, M. Grätzel, M. K. Nazeeruddin, *ChemSusChem* **2008**, *1*, 699.
[8] N. Cai, S.-J. Moon, N.-L. Cevey-Ha, T. Moehl, R. Humphry-Baker, P. Wang, S. M. Zakeeruddin, M. Grätzel, *Nano Lett.* **2011**, DOI: 10.1021/nl104034e.
[9] M. Grätzel, *MRS Bull.* **2005**, *30*, 23.
[10] H. J. Snaith, R. Humphry-Baker, P. Chen, I. Cesar, S. M. Zakeeruddin, M. Grätzel, *Nanotechnol.* **2008**, *19*, 424003.
[11] H. J. Snaith, A. J. Moule, C. Klein, K. Meerholz, R. H. Friend, M. Grätzel, *Nano Lett.* **2007**, *7*, 3372.
[12] L. Schmidt-Mende, M. Grätzel, *Thin Solid Films* **2006**, *500*, 296.
[13] I.-K. Ding, N. Tétreault, J. Brillet, B. E. Hardin, E. H. Smith, S. J. Rosenthal, F. Sauvage, M. Grätzel, M. D. McGehee, *Adv. Funct. Mater.* **2009**, *19*, 2431.
[14] I.-K. Ding, J. Melas-Kyriazi, N.-L. Cevey-Ha, K. G. Chittibabu, S. M. Zakeeruddin, M. Grätzel, M. D. McGehee, *Org. Electron.* **2010**, *11*, 1217.
[15] L. Schmidt-Mende, S. M. Zakeeruddin, M. Grätzel, *App. Phys. Lett.* **2005**, *86*, 013504.
[16] J. E. Kroeze, N. Hirata, L. Schmidt-Mende, C. Orizu, S. D. Ogier, K. Carr, M. Grätzel, J. R. Durrant, *Adv. Funct. Mater.* **2006**, *16*, 1832.
[17] U. Bach, Y. Tachibana, J.-E. Moser, S. A. Haque, J. R. Durrant, M. Grätzel, D. R. Klug, *J. Am. Chem. Soc.* **1999**, *121*, 7445.
[18] P. Wang, S. M. Zakeeruddin, J.-E. Moser, M. K. Nazeeruddin, T. Sekiguchi, M. Grätzel, *Nature Mater.* **2003**, *2*, 402.
[19] S. A. Haque, T. Park, A. B. Holmes, J. R. Durrant, *ChemPhysChem* **2003**, *4*, 89.
[20] U. Bach, Ph.D. Thesis, École Polytechnique Fédérale de Lausanne (Switzerland), **2000**.
[21] G. Boschloo, A. Hagfeldt, *Chem. Phys. Lett.* **2003**, *370*, 381.
[22] M. K. Nazeeruddin, S. M. Zakeeruddin, J.-J. Lagref, P. Liska, P. Comte, C. Barolo, G. Viscardi, K. Schenk, M. Grätzel, *Coord. Chem. Rev.* **2004**, *248*, 1317.
[23] S. Ardo, Y. Sun, A. Staniszewski, F. N. Castellano, G. J. Meyer, *J. Am. Chem. Soc.* **2010**, *132*, 6696.
[24] U. B. Cappel, S. M. Feldt, J. Schöneboom, A. Hagfeldt, G. Boschloo, *J. Am. Chem. Soc.* **2010**, *132*, 9096.
[25] U. B. Cappel, E. A. Gibson, A. Hagfeldt, G. Boschloo, *J. Phys. Chem. C* **2009**, *113*, 6275.
[26] Q. Wang, S. M. Zakeeruddin, M. K. Nazeeruddin, R. Humphry-Baker, M. Grätzel, *J. Am. Chem. Soc.* **2006**, *128*, 4446.
[27] S. N. Mori, W. Kubo, T. Kanzaki, N. Masaki, Y. Wada, S. Yanagida, *J. Phys. Chem. C* **2007**, *111*, 3522.
[28] H. J. Snaith, L. Schmidt-Mende, M. Grätzel, *Phys. Rev. B* **2006**, *74*, 045306.
[29] B. C. O'Regan, F. Lenzmann, *J. Phys. Chem. B* **2004**, *108*, 4342.
[30] N. Kopidakis, E. A. Schiff, N.-G. Park, J. v. d. Lagemaat, A. J. Frank, *J. Phys. Chem. B* **2000**, *104*, 3930.
[31] H. J. Snaith, M. Grätzel, *Adv. Mater.* **2007**, *19*, 3643.
[32] K. D. Benkstein, N. Kopidakis, J. v. d. Lagemaat, A. J. Frank, *J. Phys. Chem. B* **2003**, *107*, 7759.
[33] J. A. Chang, J. H. Rhee, S. H. Im, Y. H. Lee, H.-J. Kim, S. I. Seok, M. K. Nazeeruddin, M. Grätzel, *Nano Lett.* **2010**, *10*, 2609.
[34] X. Liu, W. Zhang, S. Uchida, L. Cai, B. Liu, S. Ramakrishna, *Adv. Mater.* **2010**, *22*, E150.
[35] P. R. F. Barnes, A. Y. Anderson, S. E. Koops, J. R. Durrant, B. C. O'Regan, *J. Phys. Chem. C* **2009**, *113*, 1126.
[36] J. Villanueva-Cab, H. Wang, G. Oskam, L. M. Peter, *J. Phys. Chem. Lett.* **2010**, *1*, 748.
[37] P. R. F. Barnes, B. C. O'Regan, *J. Phys. Chem. C* **2010**, *114*, 19134.
[38] Q. Wang, Z. Zhang, S. M. Zakeeruddin, M. Grätzel, *J. Phys. Chem. C* **2008**, *112*, 7084.
[39] G. F. Burkhard, E. T. Hoke, M. D. McGehee, *Adv. Mater.* **2010**, *22*, 3293.
[40] S. Nejati, K. K. S. Lau, *Nano Lett.* **2011**, *11*, 419.
[41] J.-H. Yum, B. E. Hardin, S.-J. Moon, E. Baranoff, F. Nüesch, M. D. McGehee, M. Grätzel, M. K. Nazeeruddin, *Angew. Chem. Int. Ed.* **2009**, *48*, 9277.
[42] K. Driscoll, J. Fang, N. Humphry-Baker, T. Torres, W. T. S. Huck, H. J. Snaith, R. H. Friend, *Nano Lett.* **2010**, *10*, 4981.
[43] B. E. Hardin, E. T. Hoke, P. B. Armstrong, J.-H. Yum, P. Comte, T. Torres, J. M. J. Fréchet, M. K. Nazeeruddin, M. Grätzel, M. D. McGehee, *Nature Photon.* **2009**, *3*, 406.
[44] I.-K. Ding, J. Zhu, W. Cai, S.-J. Moon, N. Cai, P. Wang, S. M. Zakeeruddin, M. Grätzel, M. L. Brongersma, Y. Cui, M. D. McGehee, *Adv. Energy Mater.* **2011**, *1*, 52.
[45] M. D. Brown, T. Suteewong, R. S. S. Kumar, A. P. V. D'Innocenzo, M. M. Lee, U. Wiesner, H. J. Snaith, *Nano Lett.* **2011**, *11*, 438.
[46] D. Kuang, C. Klein, H. J. Snaith, J.-E. Moser, R. Humphry-Baker, P. Comte, S. M. Zakeeruddin, M. Grätzel, *Nano Lett.* **2006**, *6*, 769.
[47] M. Wang, C. Grätzel, S.-J. Moon, R. Humphry-Baker, N. Rossier-Iten, S. M. Zakeeruddin, M. Grätzel, *Adv. Funct. Mater.* **2009**, *19*, 2163.
[48] M. K. Nazeeruddin, P. Péchy, T. Renouard, S. M. Zakeeruddin, R. Humphry-Baker, P. Comte, P. Liska, L. Cevey, E. Costa, V. Shklover, L. Spiccia, G. B. Deacon, C. A. Bignozzi, M. Grätzel, *J. Am. Chem. Soc.* **2001**, *123*, 1613.

Submitted to ADVANCED ENERGY MATERIALS

Supporting Information

for *Adv. Energy Mater.*, DOI: 10.1002/aenm.201100046

The Effect of Hole Transport Material Pore Filling on Photovoltaic Performance in Solid-State Dye-Sensitized Solar Cells

John Melas-Kyriazi, I-Kang Ding, Arianna Marchioro, Angela Punzi, Brian E. Hardin, George F. Burkhard, Nicolas Tétreault, Michael Grätzel, Jacques-E. Moser, and *Michael D. McGehee**

1. Derivation of Equation 1

In the transient absorption experiment, the hole injection efficiency (η_{hole_inj}) is obtained from taking the transient absorption signal for both the reference Z907-sensitized TiO_2 film without spiro-OMeTAD and a Z907-sensitized TiO_2 film with spiro-OMeTAD. In this section, Equation 1 in the main text will be derived.

1.1. Experiment 1: Transient Absorption in the Absence of Spiro-OMeTAD

Since there is no spiro-OMeTAD in this system, the only mechanism for the decay of dye cations is recombination with electrons in TiO_2. At steady state, the concentrations of dye and dye cation present in the system are C^0_{dye} and C^0_{dye+}, respectively. After a laser pump signal at wavelength λ_{pump}, ΔC dye molecules per unit volume that were excited by the pulse inject electrons into the TiO_2 conduction band, leaving behind dye cations.

$$C_{dye}(t) = C^0_{dye} - \Delta C \times (1 - d(t)) \quad \text{(S1)}$$

$$C_{dye+}(t) = C^0_{dye+} + \Delta C \times (1 - d(t)) \quad \text{(S2)}$$

Here, *d(t)* is the function that returns the fraction of dye cations that have recombined with electrons in TiO_2 at time τ after the laser pulse. Generally, this takes the following form (where τ is a time constant associated with the dye being used):

$$d(t) = 1 - e^{-t/\tau} \tag{S3}$$

Looking only at changes in concentration before and after the pulse, we find:

$$\Delta C_{dye}(t) = \Delta C \times (1 - d(t)) \tag{S4}$$

$$\Delta C_{dye+}(t) = \Delta C \times (1 - d(t)) \tag{S5}$$

We can directly measure ΔC in a number of ways. The easiest way is to probe at a wavelength (λ_{probe}) where the dye absorbs strongly and the dye cation barely absorbs at all. Using the Beer-Lambert law, we can relate the steady state absorbance (ie. optical density) of the film at λ_{probe} without spiro-OMeTAD (OD_{wo_spiro}) to the absorption path length (l), dye concentration, and the dye molar extinction coefficient at the probe wavelength (ε_{dye}):

$$OD_{wo\_spiro}(t) = \varepsilon_{dye} \times C_{dye}(t) \times l \tag{S6}$$

We are assuming that no other species will absorb at this wavelength, such as dye cations or electrons in TiO_2. This is a critical assumption, and must be well justified in order to maintain experimental accuracy. After a small perturbation from a pump pulse, the absorption will change:

$$\Delta OD_{wo\_spiro}(t) = \varepsilon_{dye} \times \Delta C_{dye}(t) \times l = \varepsilon_{dye} \times \left[\Delta C \times (1 - d(t))\right] \times l \tag{S7}$$

If we make this measurement at a short time after perturbation ($t = t_0$) when $d(t) \approx 0$, then:

$$\Delta C \approx \frac{-\Delta OD_{wo\_spiro}(t_0)}{l \times \varepsilon_{dye}} \tag{S8}$$

1.2. Experiment 2: Transient Absorption in the Presence of Spiro-OMeTAD

Now, we examine an identical system, but this time with spiro-OMeTAD infiltrated into the pores of the TiO_2 film. At steady state, the concentrations of dye, dye cation, and oxidized spiro-OMeTAD present in the system are C^0_{dye}, C^0_{dye+}, and C^0_{spiro+} respectively. It is important to note that we are assuming that unoxidized spiro-OMeTAD will not absorb at λ_{pump} or λ_{probe}. After the perturbation, dye cations will inject electrons into spiro-OMeTAD (creating more spiro-OMeTAD$^+$), and there will also be recombination between holes on dye cations and electrons in TiO_2 (we ignore recombination between holes in spiro-OMeTAD and electrons in TiO_2 because such processes happen on a much longer timescale):

$$C_{dye}(t) = C^0_{dye} - \Delta C \times (1 - d(t) - f(t)) \quad \text{(S9)}$$

$$C_{dye+}(t) = C^0_{dye+} + \Delta C \times (1 - d(t) - f(t)) \quad \text{(S10)}$$

$$C_{spiro+}(t) = C^0_{spiro+} + \Delta C \times f(t) \quad \text{(S11)}$$

The function *d(t)* is as before. Here, *f(t)* is a function that returns the fraction of dye cations that have been regenerated at time *t* by injecting holes into spiro-OMeTAD (creating spiro$^+$). In other words, *f(t)* is the cumulative hole injection efficiency at time *t* after injection. The total hole injection efficiency is the value of *f(t)* when there no more excess dye cations available for hole injection. The function *f(t)* is generally a constant minus a multi-exponential decay, representing various hole injection mechanisms. The change in concentrations after the perturbation will be:

$$\Delta C_{dye}(t) = -\Delta C \times (1 - d(t) - f(t)) \quad \text{(S12)}$$

$$\Delta C_{dye+}(t) = \Delta C \times (1 - d(t) - f(t)) \quad \text{(S13)}$$

$$\Delta C_{spiro+}(t) = \Delta C \times f(t) \quad \text{(S14)}$$

We are now interested in probing the absorption of this new system. Let's assume as before that the dye cation, spiro-OMeTAD, and electrons in TiO_2 do not absorb at our probe wavelength. The absorption of this film with spiro-OMeTAD (OD_{w_spiro}) will be:

$$OD_{w\_spiro}(t) = \varepsilon_{dye} \times C_{dye}(t) \times l + \varepsilon_{spiro+}(t) \times C_{spiro+}(t) \times l \quad \text{(S15)}$$

After a perturbation, we can calculate the change in absorption:

$$\Delta OD_{w\_spiro}(t) = \varepsilon_{dye} \times \Delta C_{dye}(t) \times l + \varepsilon_{spiro+}(t) \times \Delta C_{spiro+}(t) \times l \quad \text{(S16)}$$

Using Equations S12 and S14, we substitute and re-arrange Equation S16:

$$\Delta OD_{w\_spiro}(t) = \varepsilon_{dye} \times \left(-\Delta C \times \left(1 - d(t) - f(t)\right)\right) \times l + \varepsilon_{spiro+} \times \left(\Delta C \times f(t)\right) \times l \quad \text{(S17)}$$

$$\frac{\Delta OD_{w\_spiro}(t)}{l \times \varepsilon_{dye}} = -\Delta C \times \left(1 - d(t) - f(t)\right) + \frac{\varepsilon_{spiro+}}{\varepsilon_{dye}} \times \Delta C \times f(t) \quad \text{(S18)}$$

$$\frac{\Delta OD_{w\_spiro}(t)}{l \times \varepsilon_{dye}} = \Delta C \times \left(f(t) \times \left(1 + \frac{\varepsilon_{spiro+}}{\varepsilon_{dye}}\right) + d(t) - 1 \right) \quad \text{(S19)}$$

Now, let us evaluate this expression at our previously used $t = t_0$, plugging in the value of ΔC from Equation S8 and re-arranging. We obtain:

$$\frac{\Delta OD_{w\_spiro}(t_0)}{l \times \varepsilon_{dye}} = \frac{-\Delta OD_{wo\_spiro}(t_0)}{l \times \varepsilon_{dye}} \times \left(f(t_0) \times \left(1 + \frac{\varepsilon_{spiro+}}{\varepsilon_{dye}}\right) + d(t_0) - 1 \right) \quad \text{(S20)}$$

Using that $d(t_0) \approx 0$, and re-arranging, we obtain:

$$\frac{-\Delta OD_{wo\_spiro}(t_0)}{\Delta OD_{w\_spiro}(t_0)} = f(t_0) \times \left(1 + \frac{\varepsilon_{spiro+}}{\varepsilon_{dye}}\right) - 1 \quad \text{(S21)}$$

Finally, we obtain $f(t_0)$:

$$f(t_0) = \left(1 - \frac{\Delta OD_{w\_spiro}(t_0)}{\Delta OD_{wo\_spiro}(t_0)}\right) \times \left(1 + \frac{\varepsilon_{spiro+}}{\varepsilon_{dye}}\right)^{-1} \quad \text{(S22)}$$

We previously stated that the total hole injection efficiency is equal to $f(t_0)$ for some t_0 when there are no more excess dye cations available for hole injection, which would logically imply that $d(t_0) + f(t_0) = 1$. Here, this is not necessarily the case (since $d(t_0) \approx 0$ and $f(t_0) < 1$by assumption). However, it is quite plausible that at t_0, the hole injection efficiency has "saturated." This is perhaps more obvious when we remember that $f(t)$ is generally a constant minus a multi-exponential decay. If the decay constants are significantly smaller than t_0, then $f(t)$ will have saturated already by time t_0. If this is the case, we can say:

$$\eta_{hole\_inj} = \left(1 - \frac{\Delta OD_{w\_spiro}(t_0)}{\Delta OD_{wo\_spiro}(t_0)}\right) \times \left(1 + \frac{\varepsilon_{spiro+}}{\varepsilon_{dye}}\right)^{-1} \quad \text{(S23)}$$

Rearranging Equation S23 and replacing ε_{dye} with ε_{Z907}, we find:

$$\Delta OD_{w\_spiro} = \Delta OD_{wo\_spiro} \cdot (1 - \eta_{hole\_inj}) - \Delta OD_{wo\_spiro} \cdot \eta_{hole\_inj} \cdot \frac{\varepsilon_{spiro^+}}{\varepsilon_{Z907}} \quad \text{(S24)}$$

which is Equation 1 in the main text.

2. Derivation of Equation 2

Equation 2 in the main text is simplified from Equation 11 of reference [28]. In this section, the simplification process is shown step-by-step.

The original Equation 11 of reference [28] has the following form:

$$V_{oc} = \frac{\phi_B + \Delta\phi + 2\Delta E}{q} + \frac{kT}{q} \cdot \left[4\gamma r - \ln\left(\frac{40000 k_0^2 p(d_p) n(d_n) d_p d_n d^2}{I^{2(1-\beta)} g^2 (1 - e^{-\alpha d})^2}\right)\right] \quad \text{(S25)}$$

We also know that the recombination constant (k_0) has the following form (from Equation 6 in [28]):

$$k_0 = k_{rec} / I^{\beta} \exp(-2\gamma r) \exp\left(-\frac{\Delta E}{kT}\right) \quad \text{(S26)}$$

Substituting Equation S26 into Equation S25, we find:

$$V_{oc} = \frac{\phi_B + \Delta\phi + 2\Delta E}{q} + \frac{kT}{q} \cdot \left[4\gamma r - \ln\left(\frac{40000 k_{rec}^2 p(d_p) n(d_n) d_p d_n d^2}{I^{2(1-\beta)} g^2 (1-e^{-\alpha d})^2 I^{2\beta} \exp(-4\gamma r) \exp\left(-\frac{2\Delta E}{kT}\right)} \right) \right] \quad \text{(S27)}$$

Simplifying the terms and using the approximation that d_p and $d_n = d/2$, we find:

$$V_{oc} = \frac{\phi_B + \Delta\phi}{q} + \frac{kT}{q} \cdot \left[-\ln\left(\frac{10000 k_{rec}^2 p(d_p) n(d_n) d^4}{g^2 (1-e^{-\alpha d})^2 \cdot I^2} \right) \right] \quad \text{(S28)}$$

In Equation S28, ϕ_B is the built-in potential dictated by the work function differences between the two electrodes, $\Delta\phi$ is a potential shift at the dye interface, k_{rec} is the recombination rate constant in s^{-1} ($\kappa_{rec} = 1/\tau_{rec}$), p and n are the electron and hole concentration (in μm^{-3}), respectively, d_p and d_n are the average distance (in μm) between charge carriers and respective charge carrier extraction electrodes, d is the device thickness (in μm), g is the unitless charge generation efficiency from absorbed photons, α is the absorption coefficient (in μm^{-1}) of the sensitized film of thickness d, and I is the number of incident photons per unit area per unit time (in $\mu m^{-2}\ s^{-1}$).

It is important to recognize that the term inside the natural log must be dimensionless. In order to simplify the term reorganization process, we can divide each individual term by a constant with the same units. The addition of these constants will not affect the value of the V_{oc}.

$$V_{oc} = \frac{\phi_B + \Delta\phi}{q} + \frac{kT}{q} \cdot \left[-\ln\left(\frac{(10000/R_0)(k_{rec}/k_0)^2 \left(p(d_p)/p_0\right)\left(n(d_n)/n_0\right)\left(d/d_0\right)^4}{\left(g/g_0\right)^2 (1-e^{-\alpha d})^2 \cdot \left(I/I_0\right)^2} \right) \right] \quad \text{(S29)}$$

In our study, we wish to find the mathematical relationship between V_{oc} and TiO_2 film thickness (d), recombination lifetime (τ_{rec}) and average absorption coefficient of the film (α). Therefore we reorganize the terms in Equation S29 to find:

$$V_{oc} = \frac{\phi_B + \Delta\phi}{q} + \frac{kT}{q}\left[-\ln\left(\frac{(10000/R_0)\left(p(d_p)/p_0\right)\left(n(d_n)/n_0\right)}{(g/g_0)^2 (I/I_0)^2} \right) - \ln\left(\frac{(k_{rec}/k_0)^2 (d/d_0)^4}{(1-e^{-\alpha d})^2} \right) \right] \quad \text{(S30)}$$

Moreover, $\kappa_{rec} = 1/\tau_{rec}$ and $\kappa_0 = 1/\tau_0$ (with τ_{rec} and τ_0 have the units of s). Therefore we find:

$$V_{oc} = \frac{\phi_B + \Delta\phi}{q} + \frac{kT}{q}\left[-\ln\left(\frac{(10000/R_0)\left(p(d_p)/p_0\right)\left(n(d_n)/n_0\right)}{(g/g_0)^2 (I/I_0)^2} \right) \right] + \frac{kT}{q}\left[-\ln\left(\frac{(d/d_0)^4}{(\tau_{rec}/\tau_0)^2 (1-e^{-\alpha d})^2} \right) \right] \quad \text{(S31)}$$

The first two terms in Equation S31 can be treated as independent from d, τ_{rec}, and α, and can be lumped together as a voltage constant (V_0), which is to be experimentally determined. Simplifying Equation S31, we find:

$$V_{OC} = V_0 + \frac{2kT}{q}\left(\ln(\tau_{rec}/\tau_0) - 2\ln(d/d_0) + \ln(1-e^{-\alpha d})\right) \quad \text{(S32)}$$

which is Equation 2 in the main text.